Optimal light storage in atomic vapor

Nathaniel B. Phillips,[1] Alexey V. Gorshkov,[2] and Irina Novikova[1]
[1]*Department of Physics, College of William and Mary, Williamsburg, Virginia 23185, USA*
[2]*Department of Physics, Harvard University, Cambridge, Massachusetts 02138, USA*
(Received 21 May 2008; published 1 August 2008)

We study procedures for the optimization of efficiency of light storage and retrieval based on the dynamic form of electromagnetically induced transparency in hot Rb vapor. We present a detailed analysis of two recently demonstrated optimization protocols: a time-reversal-based iteration procedure, which finds the optimal input signal pulse shape for any given control field, and a procedure based on the calculation of an optimal control field for any given signal pulse shape. We verify that the two procedures are mutually consistent and that they both independently achieve the maximum memory efficiency for any given optical depth. We observe good agreement with theoretical predictions for moderate optical depths (<25), while at higher optical depths the experimental efficiency falls below the theoretically predicted values. We identify possible effects responsible for this reduction in memory efficiency.

DOI: 10.1103/PhysRevA.78.023801 PACS number(s): 42.50.Gy, 32.70.Jz, 42.50.Md

I. INTRODUCTION

The ability to store light pulses in matter and then retrieve them while preserving their quantum state is an important step in the realization of quantum networks and certain quantum cryptography protocols [1,2]. Mapping quantum states of light onto an ensemble of identical radiators (e.g., atoms, ions, solid-state emitters, etc.) offers a promising approach to the practical realization of quantum memory [3–6]. Recent realizations of storage and retrieval of single-photon wave packets [7–9], coherent states [5], and squeezed vacuum pulses [10,11] constitute an important step in demonstrating the potential of this method. However, the efficiency and fidelity of the storage must be significantly improved before practical applications become possible.

In this paper, we present a comprehensive analysis of two recently demonstrated optimization protocols [17,18] that are based on a recent theoretical proposal [12–16]. The first protocol iteratively optimizes the input pulse shape for any given control field [17], while the second protocol uses optimal control fields calculated for any given input pulse shape [18]. We experimentally demonstrate their mutual consistency by showing that both protocols yield the same optimal control-signal pairs and memory efficiencies. We also show that for moderate optical depths ($\lesssim 25$), the experimental results presented here (as well as in Refs. [17,18]) are in excellent agreement with a simple three-level theoretical model [12,14] with no free parameters; we discuss the details of the correspondence between the actual atomic system and this simple model. Lastly, we study the dependence of memory efficiency on the optical depth. We show that for higher optical depths ($\gtrsim 25$), the experimental efficiency falls below the theoretically predicted values, and we discuss possible effects, such as spin-wave decay and four-wave mixing, that may limit the experimentally observed memory efficiency.

The remainder of the paper is organized as follows. In Sec. II, we briefly summarize the three-level theory governing the two procedures for optimizing photon storage. In Sec. III, we describe our experimental system and discuss its correspondence to the three-level model. In Secs. IV and V, we present the results of experimental studies of both optimization procedures and demonstrate their consistency. In Sec. VI, we investigate the dependence of memory efficiency on the optical depth of the medium. Finally, in Sec. VII, we conclude with a summary of our results.

II. REVIEW OF THE THEORY

In this section, we briefly review the necessary concepts from the theoretical work [12,14] on which our experiments rely. We consider the propagation of a weak signal pulse with envelope $\mathcal{E}(t)$ and a strong (classical) control field with a Rabi frequency envelope $\Omega(t)$ [19] in a resonant Λ-type atomic medium under the conditions of electromagnetically induced transparency (EIT), as shown in Fig. 1(a). The control field creates a strong coupling between the signal field and a collective atomic spin excitation (spin wave) [4]. As a result, the input signal pulse gets spatially compressed and slowed down inside the atomic ensemble. The group velocity of the pulse is proportional to the control field intensity [20]:

$$v_g \approx 2|\Omega|^2/(\alpha\gamma) \ll c, \tag{1}$$

where γ is the decay rate of the optical polarization and α is the absorption coefficient (i.e., unsaturated absorption per unit length), so that αL is the optical depth of an atomic medium of length L [21].

Figure 1(b) illustrates schematically the three stages of the light storage process (writing, storage, and retrieval), while Figs. 1(c) and 1(d) show control and signal fields, respectively, during a typical experimental run. At the writing stage, a signal pulse $\mathcal{E}_{\text{in}}(t)$ is mapped onto the collective spin excitation $S(z)$ by adiabatically reducing the control field to zero. This spin wave is then preserved for some storage time τ, during which all optical fields are turned off. Finally, at the retrieval stage, the signal field $\mathcal{E}_{\text{out}}(t)$ is retrieved by turning the control field back on [3,4]. In the ideal case, the retrieved signal pulse is identical to the input pulse, provided the same constant control power is used at the writing and the retrieval stages. However, to realize this ideal storage, two conditions

 ©2008 The American Physical Society

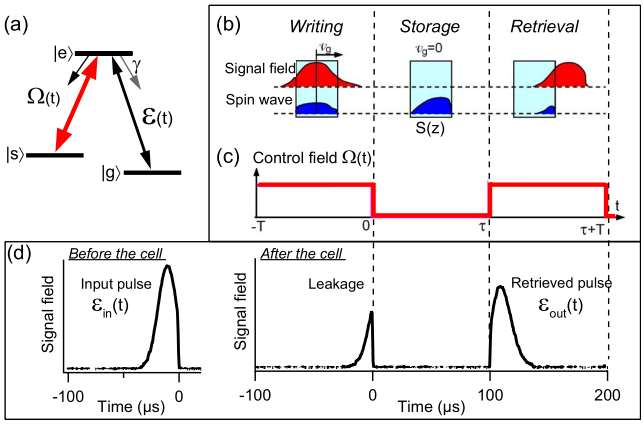

FIG. 1. (Color online) The three-level Λ scheme used in theoretical calculations (a), the schematic (b), and the example control (c) and signal (d) fields during light storage. At the writing stage ($t<0$), an input signal pulse $\mathcal{E}_{\text{in}}(t)$ propagates through the atomic medium with low group velocity v_g in the presence of a control field envelope $\Omega(t)$. While compressed inside the cell, the pulse is mapped onto a spin wave $S(z)$ by turning the control field off at time $t=0$. After a storage period τ, the spin wave is mapped back into an output signal pulse $\mathcal{E}_{\text{out}}(t)$ using the retrieval control field envelope $\Omega(t)$ $(t>\tau)$.

must be met. On the one hand, the group velocity v_g of the signal pulse inside the medium has to be low enough to spatially compress the whole pulse into the length L of the ensemble and avoid "leaking" the front edge of the pulse past the atoms. This requires $Tv_g \ll L$, where T is the duration of the incoming signal pulse. On the other hand, all spectral components of the incoming pulse must fit inside the EIT transparency window to minimize spontaneous emission losses $1/T \ll \Delta\omega_{\text{EIT}} \simeq \sqrt{\alpha L v_g/L}$ [3]. The simultaneous satisfaction of both conditions is possible only at very high optical depth $\alpha L \gg 1$ [3,12].

Experimental realization of very high optical depth in atomic ensembles requires high atomic density and/or large sample length. At high atomic density, EIT performance can be degraded by competing processes, such as stimulated Raman scattering and four-wave mixing [22–27]. Furthermore, spin-exchange collisions [28] and radiation trapping [29–31] may reduce spin-wave lifetime by orders of magnitude, limiting storage time and signal pulse durations. In addition, achieving high optical depth in some experimental arrangements may be challenging, such as in magneto-optical traps (see e.g., Refs. [8,9]). Therefore, it is crucial to be able to maximize memory efficiency by balancing the absorptive and leakage losses at moderately large αL via optimal shaping of control and/or signal temporal profiles. To characterize our memory for light, we define memory efficiency η as the probability of retrieving an incoming single photon after storage, or, equivalently, as the energy ratio between initial and retrieved signal pulses:

$$\eta = \frac{\int_{\tau}^{\tau+T} |\mathcal{E}_{\text{out}}(t)|^2 dt}{\int_{-T}^{0} |\mathcal{E}_{\text{in}}(t)|^2 dt}. \tag{2}$$

The goal of any optimization procedure is then to maximize η under the restrictions and limitations of a given system.

In the theoretical treatment of the problem, the propagation of a signal pulse in an idealized three-level Λ system, shown in Fig. 1(a), is described by three complex, dependent variables, which are functions of time t and position z [3,4,14]. These variables are the slowly varying envelope $\mathcal{E}$ of the signal field, the optical polarization P of the $|g\rangle$-$|e\rangle$ transition, and the spin coherence S. The equations of motion for these variables are [3,4,14]

$$(\partial_t + c\partial_z)\mathcal{E}(z,t) = ig\sqrt{N}P(z,t), \tag{3}$$

$$\partial_t P(z,t) = -\gamma P(z,t) + ig\sqrt{N}\mathcal{E}(z,t) + i\Omega(t-z/c)S(z,t), \tag{4}$$

$$\partial_t S(z,t) = -\gamma_s S(z,t) + i\Omega(t-z/c)P(z,t), \tag{5}$$

where $g\sqrt{N}=\sqrt{\gamma\alpha c/2}$ is the coupling constant between the atomic ensemble and the signal field, and γ and γ_s are the polarization decay rates for the transitions $|g\rangle$-$|e\rangle$ and $|g\rangle$-$|s\rangle$, respectively. While, in general, Eqs. (3)–(5) cannot be fully solved analytically, they reveal several important properties of the optimization process [12,14]. These properties are most evident in the case when spin-wave decay rate γ_s is negligible during the processes of writing and retrieval $(\gamma_s T \ll 1)$, which will hold for most of the discussion in the present paper, except for parts of Sec. VI. In this case, the highest achievable memory efficiency depends only on the optical depth αL and the mutual propagation direction of the control fields during the writing and retrieval stages [32]. For each optical depth, there exists a unique spin wave, $S_{\text{opt}}(z)$, which provides the maximum memory efficiency. Thus, the focus of the optimization process becomes identifying a matching pair of *writing* control and signal pulses that maps the signal pulse onto this optimal spin wave. Note that no additional optimization is required with respect to the *retrieval* control field, because the memory efficiency does not depend on it, provided spin-wave decay is negligible during retrieval [12,14].

In the present experiments and in Refs. [17,18], the optimization procedures were tested using weak classical signal pulses rather than quantum fields. Such experimental arrangements greatly improved the experimental simplicity and the accuracy of data analysis. At the same time, the linear equations of motion for classical and quantum signal pulses are identical, which makes the presented results applicable to quantized signal fields, such as, e.g., single photons. It is also important to note that the original theoretical work [12–16] considered a wide range of interaction processes for storing and retrieving photon wave packets (e.g., EIT, far-off-resonant Raman, and spin echo techniques) under a variety of conditions, including ensembles enclosed in a cavity [13], inhomogeneous broadening [15], and high-bandwidth nonadiabatic storage $(1/T \sim \alpha L\gamma)$ [16]. Since the proposed optimization procedures are, to a large degree, common to all interaction schemes and conditions, our results are relevant to a wide range of experimental systems.

III. EXPERIMENTAL ARRANGEMENTS

The schematic of the experimental apparatus is shown in Fig. 2. We used an external cavity diode laser (ECDL) tuned

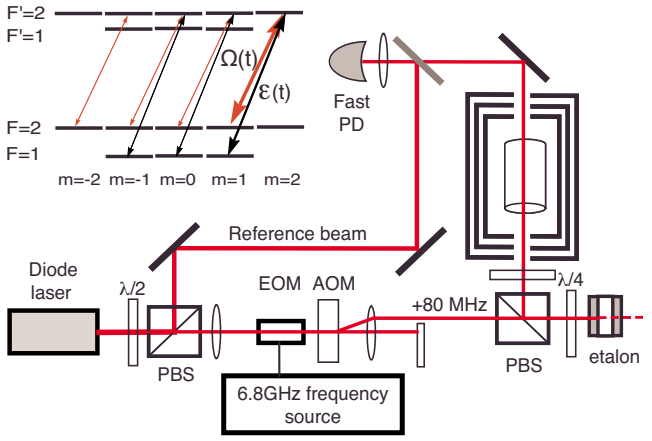

FIG. 2. (Color online) Experimental apparatus (see text for abbreviations). Inset: Schematic of the ^{87}Rb D_1 line level structure and relevant Λ systems formed by control and signal fields.

near the ^{87}Rb D_1 transition ($\lambda=795$ nm) with total available laser power ≈ 45 mW. After separating a fraction of original light for a reference beam using a polarizing beam splitter (PBS), the main laser beam passed through an electro-optical modulator (EOM), which modulated its phase at the frequency of the ground-state hyperfine splitting of ^{87}Rb ($\Delta_{\mathrm{HF}}=6.835$ GHz) and produced modulation sidebands separated by that frequency. We tuned the zeroth-order (carrier frequency) field to the $5\,^2S_{1/2}F=2\rightarrow 5\,^2P_{1/2}F'=2$ transition. This field was used as the control field during light storage. The +1 modulation sideband played the role of the signal field and was tuned to the $5\,^2S_{1/2}F=1\rightarrow 5\,^2P_{1/2}F'=2$ transition.

To carry out the optimization procedure, we had to independently manipulate the amplitudes of the control and the signal fields. We used an acousto-optical modulator (AOM) to adjust the control field intensity. However, since all optical fields traversed the AOM, the intensities of all modulation comb fields were also changed. Thus, we accordingly adjusted the rf power at the EOM input (which controls the strength of the modulation sidebands) to compensate for any changes in the signal field amplitude caused by AOM modulation.

To minimize the effects of resonant four-wave mixing, we filtered out the other (-1) first-order modulation sideband (detuned by Δ_{HF} to the red from the carrier frequency field) by reflecting the modulation comb off a temperature-tunable Fabry-Pérot étalon (Free Spectral Range=20 GHz, finesse ≈ 100). The étalon was tuned in resonance with this unwanted modulation sideband, so that most of this field was transmitted. At the same time, the control and signal field frequencies were far from the étalon resonance, and were reflected back with no losses. Such filtering allowed for suppression of the -1 modulation sideband intensity by a factor of ≈ 10.

Typical peak control field and signal field powers were 18 mW and 50 μW, respectively. The beam was weakly focused to ≈ 5 mm diameter and circularly polarized with a quarter-wave plate ($\lambda/4$). A cylindrical Pyrex cell (length and diameter were 75 and 22 mm, respectively) contained isotopically enriched ^{87}Rb and 30 Torr Ne buffer gas, so that the pressure-broadened optical transition linewidth was $2\gamma=2\pi\times 290$ MHz [33]. The cell was mounted inside three-layer magnetic shielding to reduce stray magnetic fields. The temperature of the cell was controllably varied between 45 and 75 °C using a bifilar resistive heater wound around the innermost magnetic shielding layer.

We used relatively short pulses, so that spin decoherence had a negligible effect during writing and retrieval stages (except for parts of Sec. VI) and caused only a modest reduction of the efficiency during the storage time proportional to $\exp(-2\gamma_s\tau)$. The Rb atom diffusion time out of the laser beam ($\simeq 2$ ms) was long enough to avoid diffusion-related effects on EIT dynamics [34,35]. We extracted the spin-wave decoherence time by measuring the reduction of the retrieved pulse energy as a function of storage time and fitting it to an exponential decay. We found the typical decay time to be $1/(2\gamma_s)\simeq 500$ μs, most likely arising from small, uncompensated, remnant magnetic fields.

After the cell, the output laser fields were recombined with the reference beam (at the unshifted laser frequency) at a fast photodetector, and the amplitude of each field was analyzed using a microwave spectrum analyzer. Because of the 80 MHz frequency shift introduced by the AOM, the beat note frequencies of the +1 and −1 modulation sidebands with the reference beam differed by 160 MHz, which allowed for independent measurement of the amplitude of each of these fields, as well as of the control field.

To conclude this section, we explain the direct correspondence between the experimental system and the theory based on three-level atoms [Fig. 1(a)] that we reviewed in Sec. II. The goal is to use the structure of the D_1 line of ^{87}Rb (see inset in Fig. 2) to identify the optical depth αL and the control field Rabi frequency Ω for the effective three-level system. We first solve for the ground-state population distribution after control field optical pumping of the Rb D_1 line, taking into account Doppler broadening, pressure broadening, and collisional depolarization of the excited state sublevels [28]. We find the depolarization to be fast enough (for 30 Torr Ne, $\gamma_{\mathrm{depol}}=2\pi\times 190$ MHz [36]) to ensure roughly equal populations in each of the $|F,m_F\rangle=|1,-1\rangle,|1,0\rangle,|1,1\rangle$, and $|2,2\rangle$ ground state sublevels. Given this population distribution, we calculate the optical depth αL for the signal field as a function of Rb number density. For example, we find that at 60.5 °C (Rb vapor density of 2.5×10^{11} cm^{-3}) the optical depth is $\alpha L=24.0$. Moreover, approximately 60% of this optical depth comes from atomic population of $|F,m_F\rangle=|1,1\rangle$ due to the large corresponding Clebsch-Gordan coefficient. Thus, to calculate Ω, we use the dipole matrix element of the $|F=2,m_F=1\rangle\rightarrow|F'=2,m_F=2\rangle$ transition. Approximating a transverse Gaussian laser beam profile with a uniform cylindrical beam of diameter 5 mm of the same power, we find, for example, that for the control power of 16 mW, $\Omega=2\pi\times 6.13$ MHz. Since the collisionally broadened optical transition linewidth ($2\gamma=2\pi\times 290$ MHz) is comparable to the width of the Doppler profile, the effects of Doppler broadening are negligible, making Eqs. (3)–(5) directly applicable. We note that all the theoretical modeling is done with no free parameters.

IV. SIGNAL PULSE OPTIMIZATION

One approach to the optimization of light storage is based on important time-reversal properties of photon storage that hold even in the presence of irreversible polarization decay [14]. In particular, for copropagating [32] writing and retrieval control fields, the following is true under optimized conditions (see Fig. 1): if a signal pulse $\mathcal{E}_{\text{in}}(t)$ is mapped onto a spin wave using a particular control field $\Omega(t)$ and retrieved after some storage time τ using the time-reversed control field $\Omega(\mathrm{T}-t)$, the retrieved signal pulse shape $\mathcal{E}_{\text{out}}(t)$ is proportional to the time-reversed input signal pulse $\mathcal{E}_{\text{in}}(\mathrm{T}-t)$, but attenuated due to imperfect memory efficiency. (Here and throughout the paper, control and signal envelopes are assumed to be real.) This symmetry also gives rise to an experimentally realizable iteration procedure, which, for any given writing control field, determines the optimal incoming signal pulse shape. This procedure has been first demonstrated experimentally in Ref. [17]. The present experiment was performed independently on a different (although similar) experimental setup. Therefore, in order to use this procedure in Sec. VI to study the dependence of memory efficiency on the optical depth, we verify in this section its successful performance in the present experimental setup. In addition, the implementation of iterative signal optimization in this experimental setup will allow us, in Sec. V, to compare and verify the consistency of signal and control optimizations.

The sequence of experimental steps for the iterative optimization procedure is shown in Fig. 3. The plots show the control field and the measured and simulated signal fields (solid red lines in the top panel, solid black lines, and dashed blue lines, respectively). Before each iteration, we optically pumped all atoms into the state $|g\rangle$ by applying a strong control field. We started the optimization sequence by sending an arbitrary signal pulse $\mathcal{E}_{\text{in}}^{(0)}(t)$ into the cell and storing it using a chosen control field $\Omega(t)$. In the particular case shown in Fig. 3, the group velocity was too high, and most of the input pulse escaped the cell before the control field was reduced to zero. However, a fraction of the pulse, captured in the form of a spin wave, was stored for a time period $\tau = 100\ \mu$s. We then retrieved the excitation using a time-reversed control field $\Omega(t)=\Omega(\tau-t)$ and recorded the output pulse shape $\mathcal{E}_{\text{out}}^{(0)}(t)$. For the sample sequence shown, the control fields at the writing and retrieval stages were constant and identical. This completes the initial (zeroth) iteration step. The efficiency of light storage at this step was generally low, and the shape of the output pulse was quite different from the time-reverse of the initial pulse. To create the input pulse $\mathcal{E}_{\text{in}}^{(1)}(t)$ for the next iteration step, we digitally time-reversed the output $\mathcal{E}_{\text{out}}^{(0)}(t)$ of the zeroth iteration and renormalized it to compensate for energy losses during the zeroth iteration: $\mathcal{E}_{\text{in}}^{(1)}(t) \propto \mathcal{E}_{\text{out}}^{(0)}(\tau-t)$. Then, these steps were repeated iteratively until the rescaled output signal pulse became identical to the time-reversed profile of the input pulse. As expected, the memory efficiency grew with each iteration and converged to $(43 \pm 2)\%$.

To verify that the obtained efficiency is indeed the maximum possible at this optical depth and to confirm the validity of our interpretation of the results, we compare the experimental data to numerical simulations in Fig. 3. Using the calculated optical depth and the control Rabi frequency (see Sec. III), we solve Eqs. (3)–(5) analytically in the adiabatic limit $T\alpha L\gamma \gg 1$ [14], which holds throughout this paper. There is a clear agreement between the calculated and measured lineshapes and amplitudes of the signal pulses. Also, theory and experiment converge to the optimal signal pulse shape in a similar number of iteration steps (2–3), and the experimental efficiency $[(43 \pm 2)\%]$ converged to a value close to the theoretical limit of 45% (see below).

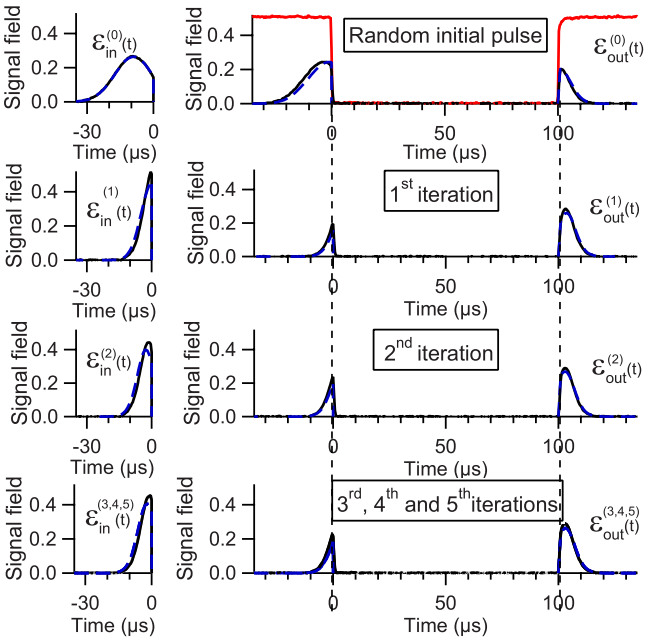

FIG. 3. (Color online) Iterative signal pulse optimization. The experimental data (solid black lines) are taken at 60.5 °C ($\alpha L = 24$) using 16 mW constant control field during writing and retrieval (solid red line in the top panel) with a $\tau = 100\ \mu$s storage interval. Numerical simulations are shown with blue dashed lines. Left: Input pulses for each iteration. Right: Signal field after the cell, showing leakage of the initial pulse for $t<0$ and the retrieved signal field $\mathcal{E}_{\text{out}}$ for $t>100\ \mu$s. Here and throughout the paper, all pulses are shown in the same scale, and all input pulses are normalized to have the same area $\int_{-\mathrm{T}}^{0}|\mathcal{E}_{\text{in}}(t)|^2 dt = 1$, where t is time in microseconds.

As in our previous study [17], we confirmed that the final memory efficiency and the signal pulse obtained after a few iteration steps were independent of the initial signal pulse $\mathcal{E}_{\text{in}}^{(0)}(t)$. We also confirmed that the optimization procedure yields the same memory efficiency for different control fields. While constant control fields of three different powers yield different optimal signal pulses [Fig. 4(a)], the measured efficiency [Fig. 4(b)] converged after a few iteration steps to the same value of $43 \pm 2\%$. With no spin-wave decay, the highest achievable memory efficiency for the optical depth $\alpha L = 24$ is 54% [14]. Taking into account spin-wave decay during the $100\ \mu$s storage time by a factor of $\exp[-100\ \mu\text{s}/500\ \mu\text{s}] = 0.82$, the highest expected efficiency is 45% [dashed line in Fig. 4(b)], which matches our experimental results reasonably well.

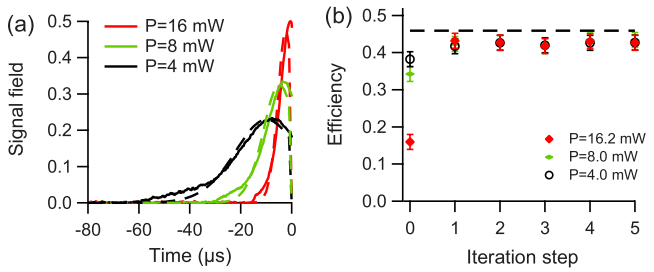

FIG. 4. (Color online) (a) Experimental (solid) and theoretical (dashed) optimized signal pulses obtained after five steps of the iteration procedure for three different powers of the constant control fields during writing and retrieval stages. (b) Corresponding memory efficiencies determined for each iteration step. Theoretically predicted optimal efficiency value is shown by the dashed line. The temperature of the cell was 60.5 °C ($\alpha L=24$).

V. CONTROL PULSE OPTIMIZATION

The iterative optimization procedure described in the previous section has an obvious advantage: the optimal signal pulse shape is found directly through experimental measurements without any prior knowledge of the system parameters (e.g., optical depth, control field Rabi frequency, various decoherence rates, etc.). However, in some situations, it is difficult or impossible to shape the input signal pulse (e.g., if it is generated by parametric down-conversion [37]). In these cases, the *control field* temporal profile must be adjusted in order to optimally store and retrieve a given signal pulse.

To find the optimal writing control field for a given input pulse shape $\mathcal{E}_{\text{in}}(t)$, we maximize η [Eq. (2)] within the three-level model [Eqs. (3)–(5)]. As explained in Sec. II, in this model, for a given optical depth αL and a given retrieval direction (coinciding with the storage direction in the present experiment [32]), there exists an optimal spin wave $S_{\text{opt}}(z)$, which gives the maximum memory efficiency. One way to calculate the control field required to map the input pulse onto this optimal spin wave is to first calculate an artificial "decayless" spin wave mode $s(z)$, which, like $S_{\text{opt}}(z)$, depends only on the optical depth and not on the shape of the incoming pulse. This "decayless" mode $s(z)$ hypothetically allows for unitary reversible storage of an arbitrary signal pulse in a semi-infinite and polarization-decay-free atomic ensemble, in which the group velocity of the pulse is still given by Eq. (1). The unitarity of the mapping establishes a one-to-one correspondence between a given input signal pulse shape $\mathcal{E}_{\text{in}}(t)$ and an optimal writing control field that maps this input pulse onto $s(z)$. The same control field maps this input pulse onto the true optimal spin wave $S_{\text{opt}}(z)$, once polarization decay and the finite length of the medium are taken into account. The details of this construction are described in Ref. [14].

As an example of control field optimization, we consider the storage of three different initial pulse shapes, shown by dotted black lines in the middle row in Fig. 5: a step with a rounded leading edge (a′), a segment of the sinc-function (b′), and a descending ramp (c′). The top row (a), (b), (c) shows the corresponding calculated optimal writing ($t<0$) control pulses. Since the shape and power of the *retrieval* control pulse do not affect the memory efficiency [12,14], we show, in the top row of Fig. 5, two retrieval control fields for each input pulse: a flat control field (dashed) and the time reverse of the writing control (solid). As expected, the flat control field (the same for all three inputs) results in the same output pulse [dashed in (a′), (b′), (c′)] independent of the input signal pulse, because the excitation is stored in the same optimal spin wave in each case. On the other hand, using the time-reversed writing control field for retrieval yields output pulses that are time-reversed (and attenuated)

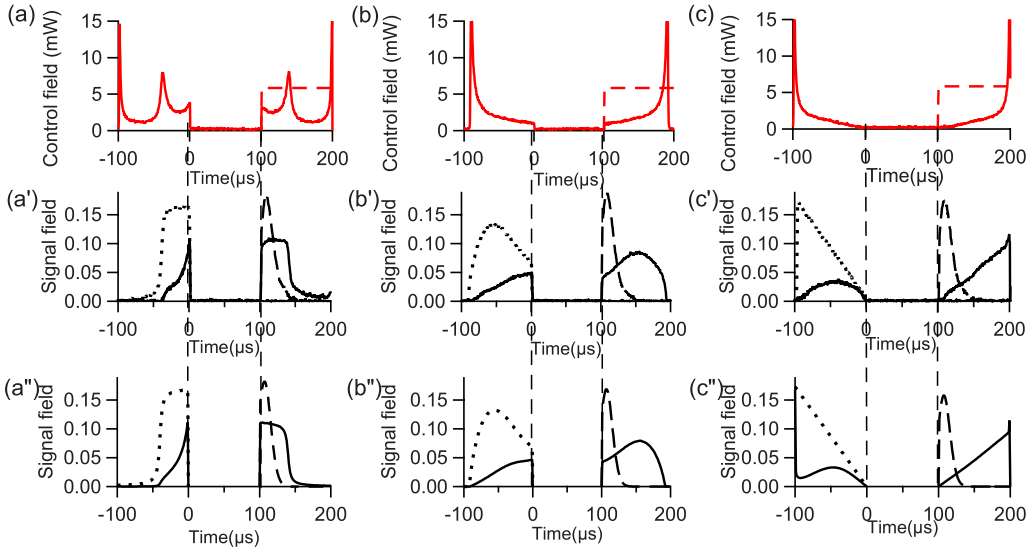

FIG. 5. (Color online) Storage of three signal pulses (a′),(b′),(c′) using calculated optimal storage ($t<0$) control fields (a), (b), (c). Input signal pulse shapes are shown in black dotted lines. The same graphs also show the leakage of the pulses (solid black lines for $t<0$) and retrieved signal pulses ($t>100$ μs) using flat control fields at the retrieval stage (dashed red lines), or using time-reversed control fields (solid red lines). Graphs (a″),(b″),(c″) show the results of numerical calculations of (a′),(b′),(c′). The temperature of the cell was 60.5 °C ($\alpha L=24$).

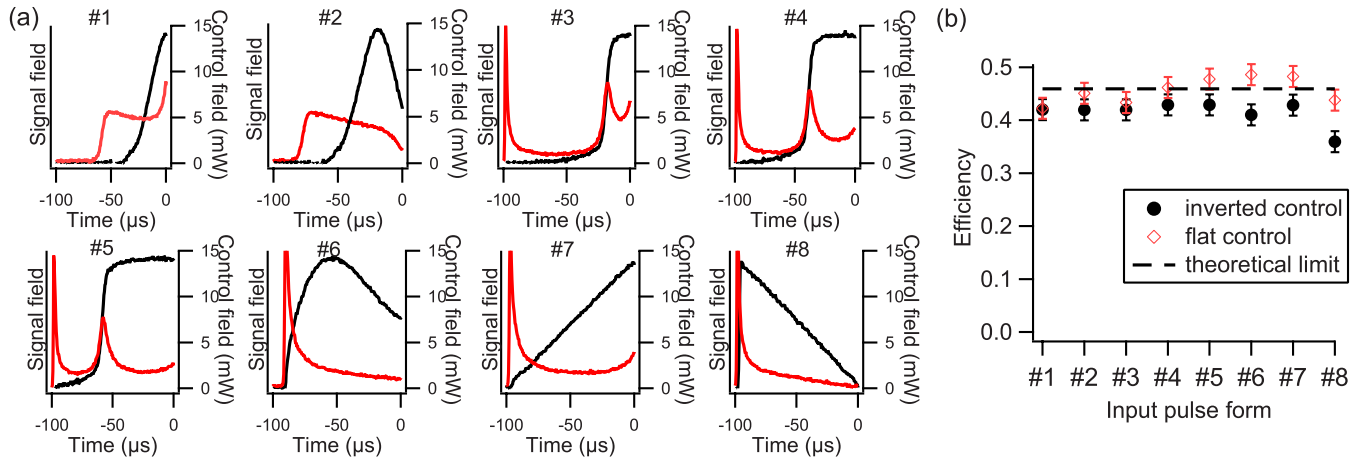

FIG. 6. (Color online) (a) Eight randomly selected signal pulse shapes (black lines) and their corresponding optimal control fields (red lines). (b) Memory efficiency for the eight signal pulse shapes using calculated optimized control fields at the writing stage, and flat control fields (open red diamonds) or inverted writing control fields (solid black circles) at the retrieval stage. Theoretically predicted optimal memory efficiency is shown by a dashed line. The temperature of the cell was 60.5 °C ($\alpha L=24$).

copies of the corresponding input pulses. This means that the time-reversal iterations of Sec. IV starting with these control-signal pairs converge on the zeroth iteration, which proves the consistency of the signal optimization of Sec. IV with the control optimization of the present section. The experimental data also agrees very well with numerical simulations [bottom row (a″), (b″), (c″) in Fig. 5], supporting the validity of our interpretation of the data.

To further test the effectiveness of the control optimization procedure, we repeated the same measurements for eight different randomly selected pulse shapes, shown as black lines in Fig. 6(a). Pulses 4, 6, and 8 are the same as the input pulses (a′), (b′), and (c′) in Fig. 5. For each of the eight input pulses, we calculated the optimal writing control [red lines in Fig. 6(a)] and then measured the memory efficiency [Fig. 6(b)], retrieving with either a constant control pulse or a time-reversed writing control pulse (open red diamonds and solid black circles, respectively). The measured efficiencies are in good agreement with each other and with the theoretically calculated maximum achievable memory efficiency of 45% (horizontal dashed line) for the given optical depth.

By performing these experiments, we found that knowledge of accurate values for the experimental parameters, such as optical depth or control field intensity, is critical for calculations of the optimal control field. Even a few percent deviation in their values caused measurable decreases in the output signal pulse amplitude. In our experiment, effective optical depth and control field Rabi frequency were computed accurately directly from measurable experimental quantities with no free parameters. The accuracy of the parameters was also verified by the excellent agreement of experimental and theoretical results of iterative optimization in Sec. IV. We note that for some other systems, the necessary experimental parameters may be difficult to compute directly with high accuracy; in that case, they can be extracted from the iteration procedure of Sec. IV.

VI. DEPENDENCE OF MEMORY EFFICIENCY ON THE OPTICAL DEPTH

In the previous two sections, we verified at optical depth $\alpha L=24$, the consistency of the signal and control optimization methods and their agreement with the three-level theory. In this section, we study the dependence of memory efficiency on optical depth. To verify the theoretical prediction that the optimal efficiency depends only on the optical depth of the sample, we repeated the iterative signal optimization procedure (Sec. IV) for several constant control field powers at different temperatures of the Rb cell ranging from 45 °C ($\alpha L=6$) to 77 °C ($\alpha L=88$). In Fig. 7(a), we plot the measured efficiencies (markers) along with the maximum achievable efficiency predicated by the theory without spin decay (thin black line) and with spin decay during the storage time (thick black line). This graph allows us to make several important conclusions.

First of all, it demonstrates that for relatively low optical depths ($\alpha L \leqslant 25$), the optimized memory efficiency for different control fields is the same, to within the experimental uncertainty, and approximately matches the theoretical value (thick black line). This confirms that the optimization procedure yields the maximum efficiency achievable for a given optical depth. However, for $\alpha L > 20$, the efficiency obtained with the lowest control field power (black empty circles) dropped below the efficiency obtained for higher control powers. As we will now show, the most probable reason for such deviation is spin-wave decay during the writing and retrieval stages.

As the optical depth increases, the duration of the optimal input pulse increases as well, as shown in Fig. 8(a), following the underlying decrease of group velocity: $T \sim L/v_g \propto \alpha L$ [14]. Thus, above a certain value of αL, the duration of the optimal pulse for a given control field becomes comparable with the spin-wave lifetime, and the spin-wave decoherence during writing and retrieval stages can no longer be ignored. Further increase of the optical depth leads to a re-

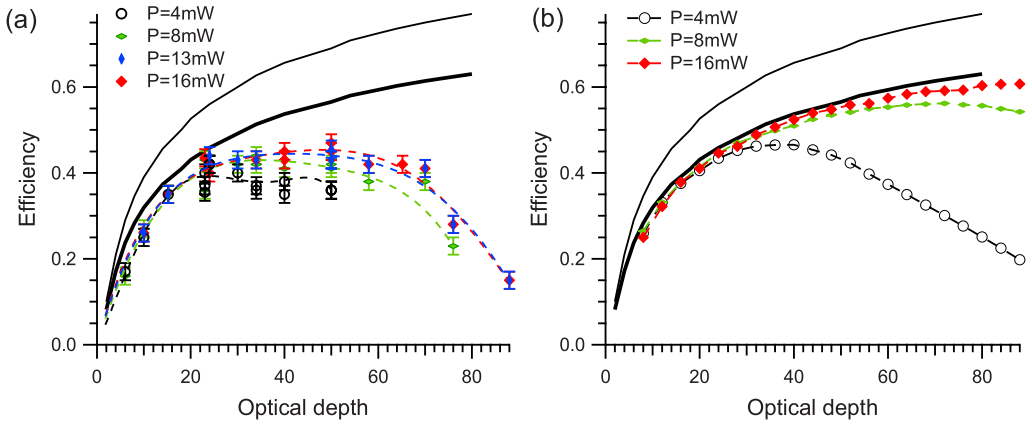

FIG. 7. (Color online) Memory efficiency as a function of optical depth obtained by carrying out iterative signal optimization until convergence. (a) At each optical depth, we considered constant control fields at four different power levels (indicated on the graph) during writing and retrieval stages. Note that many experimental data points overlap since the converged efficiencies are often the same for different control fields. Dashed lines are to guide the eye. Thin and thick black solid lines show the theoretically predicted maximum efficiency assuming no spin-wave decay and assuming an efficiency reduction by a factor of 0.82 during the 100 μs storage period, respectively. (b) Thin and thick black lines are the same as in (a), while the three lines with markers are calculated efficiencies for three different control fields (indicated on the graph) assuming spin-wave decay with a 500 μs time constant during all three stages of the storage process (writing, storage, retrieval).

duction of retrieval efficiency, even though the iterative optimization procedure is still valid [14] and produces signal pulses that are stored and retrieved with the highest efficiency possible for a given control field and αL. Figure 7(b) shows the calculated maximum achievable efficiencies for different constant control powers as a function of the optical depth, taking into account spin-wave decay with a 500 μs time constant during all three stages of light storage. For each control field power, the efficiency peaks at a certain optical depth, and then starts to decrease as optical depth increases further. Since lower control powers require longer optimal input pulses $T \sim L/v_g \propto 1/|\Omega|^2$ [see Fig. 4(a)], the corresponding efficiency reaches its peak at lower optical depths. Thus, the problem of efficiency reduction posed by

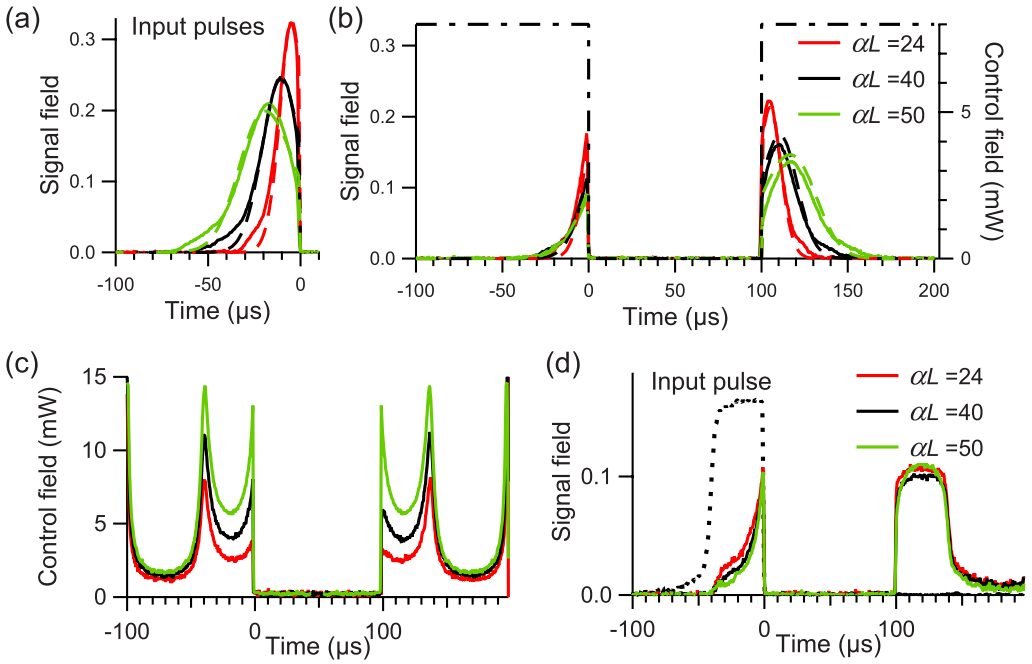

FIG. 8. (Color online) Results of the optimization procedures for different optical depths αL=24 (red), 40 (black), and 50 (green). The top panel [(a), (b)] shows storage and retrieval (b) of the optimized input signal pulses (a) obtained by running iterative optimization until convergence for a constant control field of power 8 mW [dash-dotted line in (b)]. Solid lines correspond to experimental results, while dashed lines show the results of numerical simulations. In the bottom panel [(c), (d)], (c) shows the calculated optimal writing control fields ($t<0$) for a steplike signal pulse [dotted line in (d)] and the time reverses of these control fields used during retrieval ($t>100$ μs), while (d) shows the resulting storage followed by retrieval.

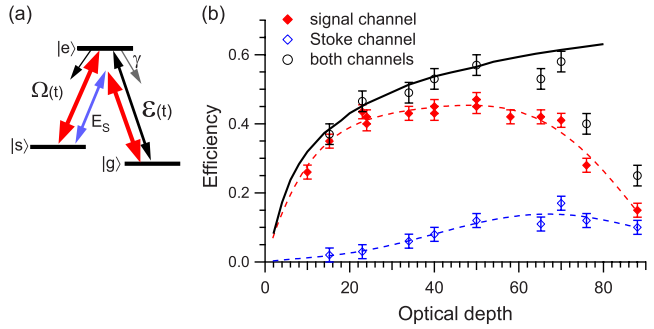

FIG. 9. (Color online) (a) Level diagram illustrating Stokes field (E_S) generation due to resonant four-wave mixing. (b) Memory efficiency for retrieval in the signal channel [same as the red filled diamonds in Fig. 7(a)], Stokes channel, and the total for both channels. The efficiencies are obtained by carrying out iterative optimization until convergence for constant writing and retrieval control fields of 16 mW power. Dashed lines are to guide the eye. The solid line (same as the thick black line in Fig. 7) shows the theoretically predicted maximum efficiency assuming an efficiency reduction by a factor of 0.82 during the 100 μs storage period.

spin-wave decay during writing and retrieval can be alleviated by using higher control powers, and hence shorter optimal signal pulses. While this effect explains the reduction of maximum memory efficiency attained with the lowest control power for $\alpha L > 20$ [Fig. 7(a)], other effects, discussed below, degrade the efficiency for all other control powers for $\alpha L > 25$, as indicated by the divergence of experimental data in Fig. 7(a) from the corresponding theoretical efficiencies in Fig. 7(b) (red and green lines). Remarkably, at these optical depths, the iterative signal optimization procedure still yields efficiencies that grow monotonically at each iteration step for the three highest control powers. This suggests that iterative signal optimization may still be yielding the optimum efficiency, although this optimum is lower than what the simple theoretical model predicts.

To further test the applicability of our optimization procedures at higher optical depths, we complemented the signal-pulse optimization [Figs. 8(a) and 8(b)] with the corresponding control field optimization [Figs. 8(c) and 8(d)]. We stored and retrieved input pulse no. 4 from Fig. 6(a) using calculated optimal writing control fields [$t < 0$ in Fig. 8(c)] at different optical depths $\alpha L = 24$, 40, and 50. As expected, the overall control power was higher at higher optical depths to keep the group velocity unchanged: $L/T \sim v_g \propto \Omega^2/(\alpha L)$. For each optical depth, we used a time-reversed writing control field to retrieve the stored spin wave. This resulted in the output signal pulse shape identical to the time-reversed (and attenuated) copy of the input pulse, as shown in Fig. 8(d). Although the memory efficiency drops below the theoretical value at these high optical depths [$\alpha L = 50$ for the green lines in Figs. 8(c) and 8(d)], the results suggest that the calculated control field may still be optimal, since it yields the time-reverse of the input signal at the output.

To gain insight into what may limit the memory efficiency for $25 < \alpha L < 60$, we investigated the effect of resonant four-wave mixing. Thus far, we have considered only the ground state coherence created by the control and signal fields in the one-photon resonant Λ configuration [Fig. 1(a)]. However, the strong control field applied to the ground state $|g\rangle$ can also generate an additional Stokes field E_S, as shown in Fig. 9(a). This process is significantly enhanced in EIT media [22,23]. In particular, it has been shown that a weak signal pulse traversing an atomic ensemble with reduced group velocity generates a complementary Stokes pulse that travels alongside with a comparably low group velocity [38,39].

To determine the effect of resonant four-wave mixing on light storage, we first carried out iterative signal optimization for a constant control field pulse of 16 mW power at different optical depths, but then detected not only the signal field, but also the Stokes field, at the retrieval stage [see Fig. 9(b)]. We see that at low optical depths, the retrieved Stokes pulse [blue empty diamonds] is negligible compared to the output signal pulse [red filled diamonds, which are the same as the red filled diamonds in Fig. 7(a)]. However, at $\alpha L \gtrsim 25$, the energy of the output pulse in the Stokes channel becomes significant. While the energy of the retrieved signal pulse stayed roughly unchanged for $25 < \alpha L < 60$, the energy of the output Stokes pulse showed steady growth with increasing αL. Moreover, the combined energy (black empty circles) of the two pulses retrieved in the signal and Stokes channels added up to match well the theoretically predicted highest achievable efficiency (solid black line). We will study elsewhere whether this match is incidental and whether it can be harnessed for memory applications. For the purposes of the present work, we simply conclude that the effects of four-wave mixing become significant around the same value of αL (~ 25) where experiment starts deviating from theory. Therefore, four-wave mixing may be one of the factors responsible for the low experimental efficiencies at high optical depths.

For $\alpha L > 60$, iterative signal optimization still converges, but efficiency does not grow monotonically at each iteration step, which clearly indicates the breakdown of time-reversal-based optimization [14]. In addition, the final efficiency is significantly lower than the theoretical value (Fig. 7). Many factors, other than four-wave mixing, may be contributing to the breakdown of time-reversal-based optimization and to the rapid decrease of memory efficiency at $\alpha L > 60$. First of all, the absorption of the control field at such high optical depths is significant (measured to be $>50\%$). In that case, the reabsorption of spontaneous radiation contributes appreciably to spin-wave decoherence [29,30] and can make the spin-wave decay rate γ_s grow with αL, reducing the light storage efficiency [31]. The spin-exchange collision rate [28], which destroys the spin-wave coherence, also becomes significant at high Rb density, reducing spin-wave lifetime even further.

VII. CONCLUSIONS

We have studied in detail two quantum memory optimization protocols in hot Rb vapor and demonstrated their consistency for maximizing memory efficiency. We have also observed good agreement between our experimental data and theoretical predictions for relatively low optical depths

(<25), both in terms of the highest memory efficiency and in terms of the optimized pulse shapes. At higher optical depths, however, the experimental efficiency was lower than predicted. We observed that resonant four-wave mixing processes became important at these higher optical depths. We expect our studies to be of importance for enhancing the performance of ensemble-based quantum memories for light.

ACKNOWLEDGMENTS

We are grateful to M. Klein, M. D. Lukin, A. S. Sørensen, and Y. Xiao for useful discussions, and to J. Goldfrank for assistance in experiments. This research was supported by National Science Foundation, Jeffress Research Grant No. J-847, and by the College of William & Mary.

[1] H. J. Briegel, W. Dur, S. J. van Enk, J. I. Cirac, and P. Zoller in *The Physics of Quantum Information*, edited by D. Bouwmeester, A. Ekert, and A. Zeilinger (Springer, Berlin, 2000), pp. 281–293.
[2] L. M. Duan, M. D. Lukin, J. I. Cirac, and P. Zoller, Nature (London) **414**, 413 (2001).
[3] M. Fleischhauer and M. D. Lukin, Phys. Rev. Lett. **84**, 5094 (2000); Phys. Rev. A **65**, 022314 (2002).
[4] M. D. Lukin, Rev. Mod. Phys. **75**, 457 (2003).
[5] B. Julsgaard *et al.*, Nature (London) **432**, 482 (2004).
[6] B. Kraus, W. Tittel, N. Gisin, M. Nilsson, S. Kroll, and J. I. Cirac, Phys. Rev. A **73**, 020302(R) (2006).
[7] M. D. Eisaman *et al.*, Nature (London) **438**, 837 (2005).
[8] T. Chanelière *et al.*, Nature (London) **438**, 833 (2005).
[9] K. S. Choi, H. Deng, J. Laurat, and H. J. Kimble, Nature (London) **452**, 67 (2008).
[10] J. Appel, E. Figueroa, D. Korystov, M. Lobino, and A. I. Lvovsky, Phys. Rev. Lett. **100**, 093602 (2008).
[11] K. Honda, D. Akamatsu, M. Arikawa, Y. Yokoi, K. Akiba, S. Nagatsuka, T. Tanimura, A. Furusawa, and M. Kozuma, Phys. Rev. Lett. **100**, 093601 (2008).
[12] A. V. Gorshkov, A. André, M. Fleischhauer, A. S. Sørensen, and M. D. Lukin, Phys. Rev. Lett. **98**, 123601 (2007).
[13] A. V. Gorshkov, A. André, M. D. Lukin, and A. S. Sørensen, Phys. Rev. A **76**, 033804 (2007).
[14] A. V. Gorshkov, A. André, M. D. Lukin, and A. S. Sørensen, Phys. Rev. A **76**, 033805 (2007).
[15] A. V. Gorshkov, A. André, M. D. Lukin, and A. S. Sørensen, Phys. Rev. A **76**, 033806 (2007).
[16] A. V. Gorshkov, T. Calarco, M. D. Lukin, and A. S. Sørensen, Phys. Rev. A **77**, 043806 (2008).
[17] I. Novikova, A. V. Gorshkov, D. F. Phillips, A. S. Sørensen, M. D. Lukin, and R. L. Walsworth, Phys. Rev. Lett. **98**, 243602 (2007).
[18] I. Novikova, N. B. Phillips, and A. V. Gorshkov, e-print arXiv:0805.1927.
[19] As in Refs. [3,12], we define the Rabi frequency Ω as $|\Omega|^2 = \wp_{es}^2 I/(2\hbar^2 \epsilon_0 c)$, where I is the control intensity.
[20] M. Fleischhauer, A. Imamoglu, and J. P. Marangos, Rev. Mod. Phys. **77**, 633 (2005).
[21] Throughout the paper, we use the traditional definition of the optical depth of a sample as the *intensity* attenuation $\exp(-\alpha L)$ of a weak resonant signal field with no control field. This definition differs by a factor of 2 from the optical depth d defined in [12–16] as the *amplitude* attenuation of a weak resonant signal field. There the intensity attenuation was given by $\exp(-2d)$, so that the two optical depth definitions are related by $\alpha L = 2d$.
[22] M. D. Lukin, M. Fleischhauer, A. S. Zibrov, H. G. Robinson, V. L. Velichansky, L. Hollberg, and M. O. Scully, Phys. Rev. Lett. **79**, 2959 (1997).
[23] M. D. Lukin, P. R. Hemmer, M. Löffler, and M. O. Scully, Phys. Rev. Lett. **81**, 2675 (1998).
[24] H. Kang, G. Hernandez, and Y. Zhu, Phys. Rev. A **70**, 061804(R) (2004).
[25] V. Wong, R. S. Bennink, A. M. Marino, R. W. Boyd, C. R. Stroud, and F. A. Narducci, Phys. Rev. A **70**, 053811 (2004).
[26] K. I. Harada, T. Kanbashi, M. Mitsunaga, and K. Motomura, Phys. Rev. A **73**, 013807 (2006).
[27] G. S. Agarwal, T. N. Dey, and D. J. Gauthier, Phys. Rev. A **74**, 043805 (2006).
[28] W. Happer, Rev. Mod. Phys. **44**, 169 (1972).
[29] A. B. Matsko, I. Novikova, M. O. Scully, and G. R. Welch, Phys. Rev. Lett. **87**, 133601 (2001).
[30] A. B. Matsko, I. Novikova, and G. R. Welch, J. Mod. Opt. **49**, 367 (2002).
[31] M. Klein, Y. Xiao, A. V. Gorshkov, M. Hohensee, C. D. Leung, M. R. Browning, D. F. Phillips, I. Novikova, and R. L. Walsworth, Proc. SPIE **6904**, 69040C1 (2008).
[32] The present experiment used copropagating writing and retrieval control fields, which correspond to "forward retrieval," using the terminology of Refs. [12–16]. Although backward retrieval is more efficient than forward retrieval for degenerate lower levels $|s\rangle$ and $|g\rangle$ of the Λ system [12,14], for the present experiment the hyperfine splitting between $|s\rangle$ and $|g\rangle$ makes forward retrieval more efficient [14].
[33] M. D. Rotondaro and G. P. Perram, J. Quant. Spectrosc. Radiat. Transf. **57**, 497 (1997).
[34] I. Novikova, Y. Xiao, D. F. Phillips, and R. L. Walsworth, J. Mod. Opt. **52**, 2381 (2005).
[35] Y. Xiao, I. Novikova, D. F. Phillips, and R. L. Walsworth, Phys. Rev. Lett. **96**, 043601 (2006).
[36] M. D. Rotondaro and G. P. Perram, Phys. Rev. A **58**, 2023 (1998).
[37] J. S. Neergaard-Nielsen, B. M. Nielsen, H. Takahashi, A. I. Vistnes, and E. S. Polzik, Opt. Express **15**, 7940 (2007).
[38] E. E. Mikhailov, Yu. V. Rostovtsev, and G. R. Welch, J. Mod. Opt. **50**, 2645 (2003).
[39] V. Boyer, C. F. McCormick, E. Arimondo, and P. D. Lett, Phys. Rev. Lett. **99**, 143601 (2007).